A model for active elements in cochlear biomechanics

S. T. Neely
Boys Town National Institute for Communication Disorders in Children, 555 North 30th Street, Omaha, Nebraska 68131

D. O. Kim
Department of Neurophysiology, University of Wisconsin, Madison, Wisconsin 53706

(Received 11 September 1985; accepted for publication 4 January 1986)

A linear, mathematical model of cochlear biomechanics is presented in this paper. In this model, active elements are essential for simulating the high sensitivity and sharp tuning characteristic of the mammalian cochlea. The active elements are intended to represent the motile action of outer hair cells; they are postulated to be mechanical force generators that are powered by electrochemical energy of the cochlear endolymph, controlled by the bending of outer hair cell stereocilia, and bidirectionally coupled to cochlear partition mechanics. The active elements are spatially distributed and function collectively as a cochlear amplifier. Excessive gain in the cochlear amplifier causes spontaneous oscillations and thereby generates spontaneous otoacoustic emissions.

PACS numbers: 43.63.Bq, 43.63.Kz

LIST OF SYMBOLS

BM	basilar membrane
CP	cochlear partition
IHC	inner hair cell
OC	organ of Corti
OHC	outer hair cell
RL	reticular lamina
ST	scala tympani
SV	scala vestibuli
TM	tectorial membrane
$P_d(x)$	pressure difference across BM (dyn · cm^{-2})
$P_a(x)$	pressure source in OHC (dyn · cm^{-2})
P_s	pressure at stapes (dyn · cm^{-2})
P_r	pressure at round window (dyn · cm^{-2})
P_e	sound pressure at eardrum (dyn · cm^{-2})
$\xi_p(x)$	average z displacement of CP over width of CP (cm)
$\xi_b(x)$	maximum z displacement of BM over width of BM (cm)
$\xi_c(x)$	shear displacement between TM and RL (cm)
$\xi_t(x)$	component of ξ_c due to TM displacement (cm)
ξ_h	fluid displacement through helicotrema (cm)
Z_m	impedance of middle ear (dyn · s · cm^{-3})
$Z_p(x)$	partition impedance (dyn · s · cm^{-3})
$Z_1(x)$	impedance associated with ξ_b (dyn · s · cm^{-3})
$Z_2(x)$	impedance associated with ξ_t (dyn · s · cm^{-3})
$Z_3(x)$	impedance associated with ξ_c (dyn · s · cm^{-3})
$Z_4(x)$	impedance associated with P_a (dyn · s · cm^{-3})
$k_1(x)$	stiffness component of Z_1 (dyn · cm^{-3})
$c_1(x)$	damping component of Z_1 (dyn · s · cm^{-3})
$m_1(x)$	mass component of Z_1 (g · cm^{-2})
$k_2(x)$	stiffness component of Z_2 (dyn · cm^{-3})
$c_2(x)$	damping component of Z_2 (dyn · s · cm^{-3})
$m_2(x)$	mass component of Z_2 (g · cm^{-2})
$k_3(x)$	stiffness component of Z_3 (dyn · cm^{-3})
$c_3(x)$	damping component of Z_3 (dyn · s · cm^{-3})
$k_4(x)$	stiffness component of Z_3 (dyn · cm^{-3})
$c_4(x)$	damping component of Z_3 (dyn · s · cm^{-3})
c_h	fluid damping at helicotrema (dyn · s · cm^{-3})
γ	OHC force-generation gain (dyn · cm^{-3})
ω	frequency (rad · s)
f	frequency (cyc · s)
L	length of SV and ST in x dimension (cm)
H	height of SV and ST in y dimension (cm)
W	width of SV and ST in z dimension (cm)
A_s	Area of stapes footplate (cm^2)
b	ratio of ξ_b to ξ_p
Δ	thickness of cross-sectional element of cochlea (cm)
N	number of spatial points used to represent cochlea in the x dimension
i	unit imaginary
π	3.14159... .
g	BM to IHC lever gain
G_m	middle ear lever gain
ρ	density of cochlear fluid (dyn · cm^{-3})

INTRODUCTION

The cochlea not only transduces mechanical vibrations into neural spike discharges, it also provides spatial separation of frequency information. This spatial frequency analysis is accomplished mechanically by means of tuned elements in the cochlear partition. Many details about how the cochlea performs frequency analysis and how it detects sounds at the threshold of hearing are still unknown. One view is that active elements in the cochlear partition provide the cochlea with the ability to amplify sounds in a frequency and place specific manner. (Davis, 1983; Kim *et al.*, 1980; Neely and Kim, 1983).

Although mathematical models have been used for

 0001-4966/86/051472-09$00.80 © 1986 Acoustical Society of America

many years to describe cochlear mechanics (Allen, 1977; de Boer, 1980, 1984; Neely, 1981, 1985; Zwislocki, 1950), a "complete" description of cochlear mechanics is not yet possible. One objective of modeling research is to design an idealized mechanical system that resembles the cochlea as much as possible, but is also simple enough to provide insight and be studied mathematically. The model of cochlear mechanics presented in this paper is based on physical principles, anatomical characteristics, and observable responses of the cochlea.

In this paper we describe the mathematical formulation of a cochlear model in one spatial dimension and compare numerical solutions with *in vivo* measurements. The emphasis in this model is on demonstrating the mechanical characteristics that are required of the cochlear partition. Within the context of this model, we find that active elements must be present in the cochlear partition to simulate basilar membrane motion that is similar to optimal *in vivo* observations (Neely and Kim, 1983). These active elements are, in effect, mechanical force generators that are controlled by basilar membrane motion and contribute energy to cochlear mechanics at the expense of electrochemical energy. The active elements in the present model take the form of *pressure sources* located within the outer hair cells.

We show how a decrease in the gain parameter of the active elements leads to loss of tuning and sensitivity in the model in a manner similar to that observed *in vivo* as the animal's physiological condition deteriorates. Although our model solutions are stable for our simulation of normal cochlear mechanics (in the sense that transient responses decay with time), we show that larger gain values can cause spontaneous oscillations and generate spontaneous otoacoustic emissions.

I. MACROMECHANICS

Most of the usual assumptions are made about cochlear macromechanics (e.g., Viergever, 1980). The cochlea is represented as a fluid-filled box that is divided into upper and lower chambers by a flexible partition. The cochlear fluid is modeled as inviscid and incompressible. The basal boundary of the cochlear box is located at the origin of a three-dimensional coordinate system as illustrated in Fig. 1. The x dimension describes the length of the cochlea, the y dimension the width, and the z dimension the height. The upper half of the box is called the scala vestibuli (SV), the lower half of the box is called the scala tympani (ST), and the separation between the upper and lower halves is called the cochlear partition (CP).

Equations describing cochlear macromechanics are formulated in terms of fluid pressure and acceleration of the sides of the box. We will define $P_d(x)$ as the difference in fluid pressure across both the partition and the cochlear fluid that "rides" with the partition (Neely, 1985). Positive values of $P_d(x)$ will generate a force on the partition in the positive z direction. The displacement of the partition in the z direction, averaged over the width of the partition, is $\xi_p(x)$. A one-dimensional approximation of cochlear fluid mechanics can be written as

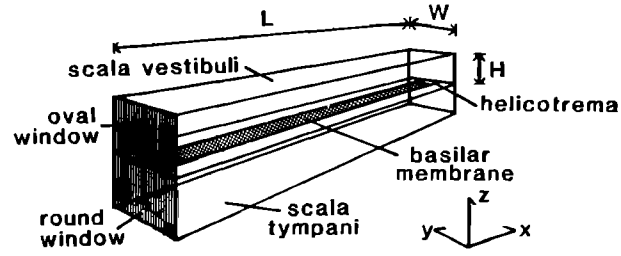

FIG. 1. Box model of the cochlea. The cochlea is represented as a fluid-filled box which is divided into upper and lower halves by a flexible partition. A three-dimensional coordinate system is defined with its origin at the basal end of the cochlear partition. The x dimension describes the length of the cochlea, the y dimension the width, and the z dimension the height. Signal input to the cochlea is provided by the footplate of the stapes which occupies the oval window. Displacement of the round window is equal and opposite to that of the oval window due to incompressibility of the fluid.

$$\frac{d^2}{dx^2}P_d(x) = \frac{2\rho}{H}\ddot{\xi}_p(x), \tag{1}$$

where ρ is the fluid density and the double-dot notation indicates two time derivatives. At the basal and apical ends of the cochlea we will use the following boundary conditions:

$$\frac{d}{dx}P_d(0) = 2\rho\ddot{\xi}_s, \tag{2}$$

$$\frac{d}{dx}P_d(L) = 2\rho\ddot{\xi}_h, \tag{3}$$

where ξ_s represents inward displacement of the stapes footplate and ξ_h represents displacement of fluid from SV to ST through the helicotrema.

In a frequency-domain formulation with assumed $e^{i\omega t}$ time dependence, each of the displacement variables ξ_p, ξ_s, and ξ_h can be eliminated from the above equations by introducing the appropriate mechanical impedance functions. We will assume that our stimulus is specified in terms of sound pressure at the eardrum P_e. If $Z_m = k_m/i\omega + c_m + i\omega m_m$ is the impedance of the middle ear (Guinan and Peake, 1967; Lynch *et al.*, 1981) then we can express stapes acceleration as

$$\ddot{\xi}_s = (i\omega/Z_m)[(A_m/G_m A_s)P_e - P_d(0)], \tag{4}$$

where A_m is the effective area of the eardrum, A_s is the effective area of the stapes, and G_m is the lever gain of the middle ear. We assume that fluid motion through the helicotrema is opposed by viscous damping c_h, so that

$$\ddot{\xi}_h = (i\omega/c_h)P_d(L). \tag{5}$$

The partition impedance $Z_p(x)$ describes the (bidirectional) coupling between the macromechanics of the fluid and the micromechanics of the organ of Corti,

$$\ddot{\xi}_p(x) = [i\omega/Z_p(x)]P_d(x). \tag{6}$$

By substituting Eqs. (4)–(6) into Eqs. (1)–(3) we obtain a frequency-domain formulation of the one-dimensional model expressed in terms of fluid pressure $P_d(x)$.

II. MICROMECHANICS

The model of cochlear micromechanics presented in this section represents an attempt to bridge the gap between what we know about mechanical properties of the sensory hair cells and signal processing capabilities of the cochlea. To solve for cochlear macromechanics we need to describe the micromechanics of the cochlear partition in terms of the partition impedance $Z_p(x)$. To compare model solutions with *in vivo* measurements, we also need an explicit representation for organ of Corti (OC) displacement ξ_b and sensory hair cell excitation ξ_c.

We assume that the CP is always displaced in the same shape (bending mode) which is independent of x. If we define b as the ratio of the average displacement across the width of the CP $\dot{\xi}_p$ to the maximum displacement over the width of the BM $\dot{\xi}_b$, then for any given position

$$\xi_p(x) = b\xi_b(x). \tag{7}$$

By this definition the value of b is always less than one.

Mechanical excitation to the sensory hair cells (both inner and outer hair cells) is assumed to be due to the relative shearing displacement between the tectorial membrane (TM) and the reticular lamina (RL) (see Fig. 2). We define ξ_c to be the difference between two radially oriented displacements,

$$\xi_c(x) = g(x)\xi_b(x) - \xi_t(x), \tag{8}$$

where $g(x)$ is the lever gain between the OC displacement ξ_b and the radial displacement of the RL and ξ_t is the radial motion of the TM (Rhode and Geisler, 1967). We will use $\dot{\xi}_c$ to describe the hair bundle displacement of both inner and outer hair cells. At the outer hair cells (OHC) we assume that $\dot{\xi}_c$ the mechanical force generator is internal to the OHC. At the inner hair cells (IHC) we assume that neural rate threshold occurs at a constant peak displacement of $\dot{\xi}_c$.

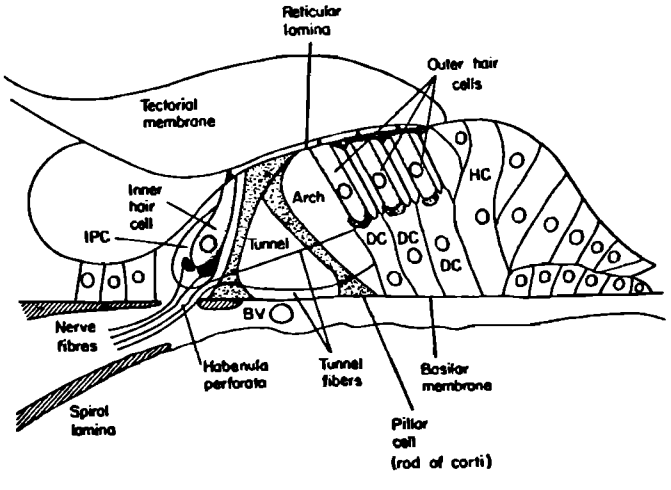

FIG. 2. Cross-sectional view of the organ of Corti. The anatomical components of the organ of Corti form the basis for cochlear micromechanics. Fluid pressure difference across organ of Corti causes vertical displacement of the basilar membrane and a proportional radial shear displacement between the reticular lamina and the tectorial membrane. [From Pickles (1982) with permission of the author and publisher.]

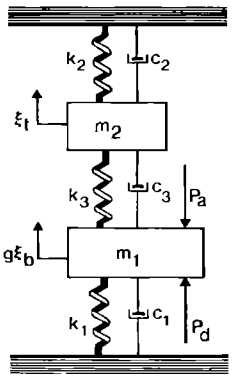

FIG. 3. Lumped component model of cochlear micromechanics. The mass m_1 represents a cross section of the organ of Corti (OC) which is attached to rigid bone by stiffness and damping components k_1 and c_1. The BM is "driven" by fluid pressure difference P_d and active pressure source P_a. The mass m_2 represents a cross section of the tectorial membrane (TM) which is attached to rigid bone by k_2 and c_2. The two masses are coupled by k_3 and c_3. The relative motion between BM and TM represents hair bundle displacement ξ_c.

In the model, OC and TM are mechanically coupled and driven by both fluid pressure and a pressure source due to mechanical force generated by the OHC as illustrated schematically in Fig. 3. Our micromechanical model has two mechanical degrees-of-freedom (DOF) at each position x; each DOF contributes a component to the radially oriented shearing displacement between the RL and the TM. In the frequency domain, our equation of motion for first DOF is

$$P_d(x) - P_a(x) = gZ_1(x)\dot{\xi}_b(x) + Z_3(x)\dot{\xi}_c(x), \tag{9}$$

where $Z_1 = k_1/i\omega + c_1 + i\omega m$, represents the mechanical impedance of the OC, $Z_2 = k_2/i\omega + c_2 + i\omega m_2$ represents the mechanical impedance of the TM, and P_a is a pressure source located within the OHC (see Fig. 3). Our equation of motion for the second DOF is

$$0 = Z_2(x)\dot{\xi}_t(x) - Z_3(x)\dot{\xi}_c(x), \tag{10}$$

where $Z_3 = k_3/i\omega + c_3$ represents the coupling between OC and TM.

The pressure source P_a is not an independent source in this model; it is controlled by sensory cell displacement ξ_c in a manner consistent with *in vitro* observations of hair cells. A vestibular hair cell is depolarized when its hair bundle is pushed toward its tallest stereocillium (Hudspeth and Corey, 1977). For the OHC in our model the hair bundle is pushed in the depolarizing direction when ξ_c increases. *In vitro* observation of OHC motility indicates that the height of the OHC decreases when the cell is depolarized (Brownell *et al.*, 1985). We interpret this shortening of OHC height to be the result of an internal pressure decrease in the OHC. In terms of our model, this means that (for low-frequency stimuli) the pressure inside the OHC should decrease when ξ_c increases. Because the fluid surrounding the OHC is incompressible, internal pressure changes are transmitted *isometrically* to the surrounding fluid. With these observations in mind, we define the pressure source by

$$P_a(x) = -\gamma Z_4(x)\dot{\xi}_c(x), \tag{11}$$

where γ is a *gain control* on the active element and $Z_4 = k_4/i\omega + c_4$ is included to provide a frequency-dependent phase *shift between* P_a and ξ_c. It should be noted that γ is independent of x and ω by definition and will be used only to demonstrate the effects on the model of *global* changes in the active elements.

The driving-point impedance of the CP can now be expressed as

$$Z_p = (g/b)[Z_1 + Z_2(Z_3 - \gamma Z_4)/(Z_2 + Z_3)]. \quad (12)$$

After solving the macromechanical equations for P_d, the displacement variables ξ_b and ξ_c are obtained by the following equations:

$$\xi_b = P_d/i\omega b Z_p, \quad (13)$$

$$\xi_c = [gZ_2/(Z_2 + Z_3)]\xi_b. \quad (14)$$

It should be noted that Eq. (14) defines a "second filter" of the same form as that proposed by Allen (1980) and Zwislocki and Kletsky (1979a,b) The major difference between our micromechanical model and their "second filter" models is the presence of the pressure source P_a. This *active element* in our model is represented in Eq. (12) by "negative damping" regions in the partition impedance Z_p which supply energy to the cochlear fluid in a manner which is both frequency and place specific.

III. MODEL RESULTS

The cochlear model described above was solved numerically using methods outlined in the Appendix for model parameters listed in Table I. The model parameters were selected to simulate the biomechanics of a cat cochlea with consideration given to the physical structure, frequency-to-place map, and frequency tuning curves typical for a cat.

In Figs. (4)–(6) we show the distribution of pressure P_d, basilar membrane displacement ξ_b, and hair cell excitation ξ_c, as a function of distance from the stapes for four frequencies: 0.4, 1.6, 6.4, and 25.6 kHz assuming a stimulus level of 0 dB SPL at the eardrum. We define the characteristic place for a given frequency as the x position corresponding to the maximum of $|\xi_c(x)|$. Note that the tuning of

TABLE I. Model parameters values (cgs units).

$k_1(x)$	$1.1 \cdot 10^9 e^{-4x}$ dyn · cm^{-3}
$c_1(x)$	$20 + 1500 e^{-2x}$ dyn · s · cm^{-3}
$m_1(x)$	$3 \cdot 10^{-3}$ g · cm^{-2}
$k_2(x)$	$7 \cdot 10^6 e^{-4.4x}$ dyn · cm^{-3}
$c_2(x)$	$10 e^{2.2x}$ dyn · s · cm^{-3}
$m_2(x)$	$0.5 \cdot 10^{-3} e^{x}$ g · cm^{-2}
$k_3(x)$	$10^7 e^{-4x}$ dyn · cm^{-3}
$c_3(x)$	$2 e^{-0.8x}$ dyn · s · cm^{-3}
$k_4(x)$	$6.15 \cdot 10^8 e^{-4x}$ dyn · cm^{-3}
$c_4(x)$	$1040 e^{-2x}$ dyn · s · cm^{-3}
γ	1 dyn · cm^{-3}
g	1
b	0.4
L	2.5 cm
H	0.1 cm
W	0.1 cm
k_m	$2.1 \cdot 10^5$ dyn · cm^{-3}
c_m	400 dyn · s · cm^{-3}
m_m	$45 \cdot 10^{-3}$ g · cm^{-2}
A_s	0.01 cm^2
A_m	0.35 cm^2
G_m	0.5
N	251
ρ	1 dyn · cm^{-3}

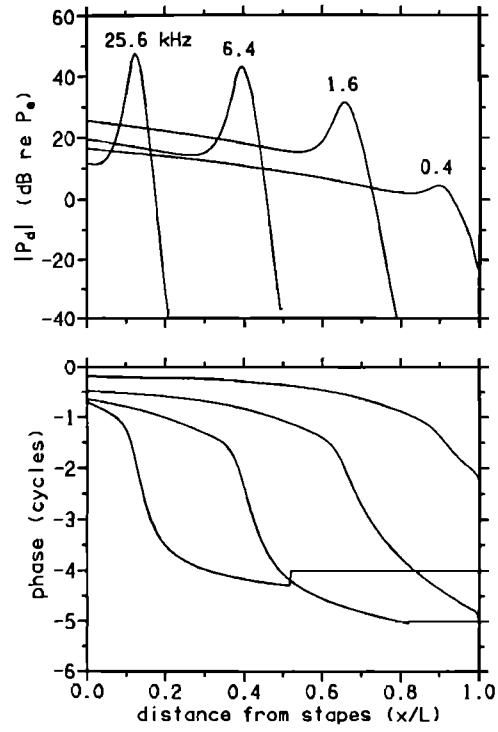

FIG. 4. Pressure difference across the cochlear partition P_d as a function of x in the model. In this figure and the next two figures the curves represent four solutions of the cochlear model for four frequencies: 0.4, 1.6, 6.4, and 25.6 kHz. The magnitude and phase of P_d are plotted relative to sound pressure at the eardrum P_e

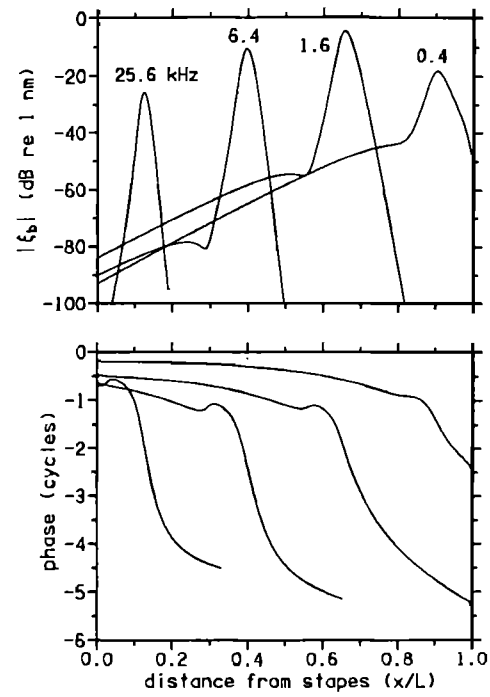

FIG. 5. Basilar membrane displacement ξ_b as a function of x in the model. The magnitude is plotted in dB *re*: 1 nm with eardrum pressure at 0 dB SPL [*re*: 2×10^{-5} N · m^{-2} (rms) = 2.848×10^{-4} dyn · cm^{-2} (peak)].

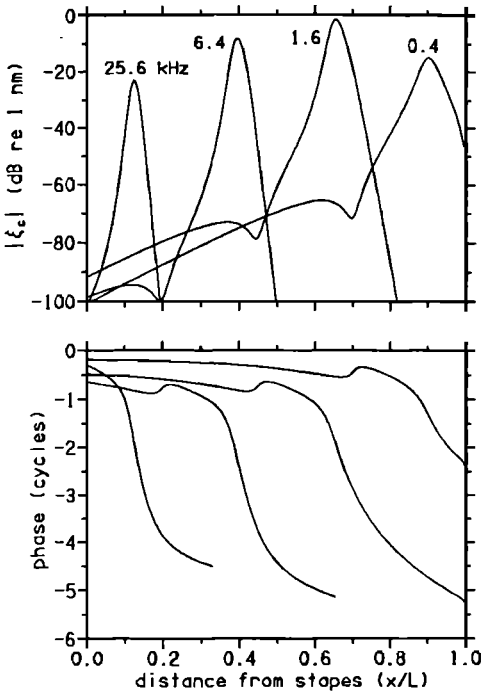

FIG. 6. Hair bundle displacement ξ_c as a function of x in the model. The magnitude is plotted in dB *re*: 1 nm with eardrum pressure at 0 dB SPL.

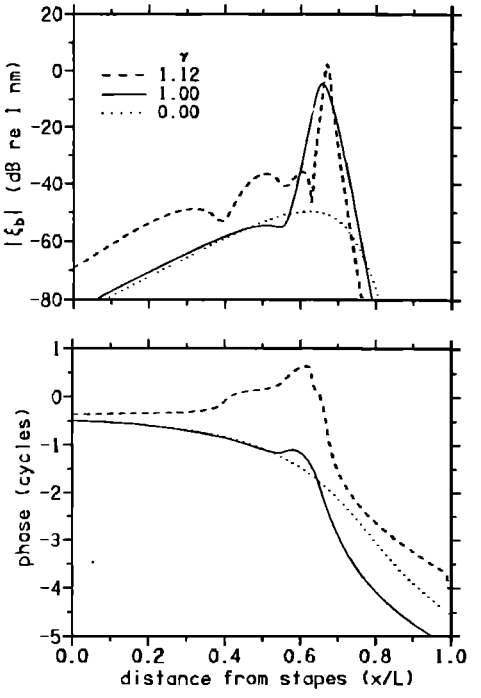

FIG. 7. Effect on basilar membrane displacement ξ_b due to changes in transduction gain γ. The dotted line represents a "passive" cochlea with $\gamma = 0$, the solid line represents a "normal" cochlea with $\gamma = 1$, and the dashed line represents an "unstable" cochlea with $\gamma = 1.12$.

$|\xi_c(x)|$ near the characteristic place for each frequency in Fig. 6 is primarily determined by a peak in the pressure P_d as seen in Fig. 4. The stiffness of the basilar membrane (BM) provides attenuation of BM displacement on the basal side of the characteristic place in Fig. 5. Some further increase in the tip-to-tail ratio is provided to $|\xi_c(x)|$ in Fig. 6 by the frequency-dependent influence of the tectorial membrane.

The effect of the active elements on basilar membrane response is clearly shown by solutions for different values of the OHC force-generation gain parameter γ. In Fig. 7, solutions of the model at 1.6 kHz for three values of γ are shown: the dotted line represents a passive model with $\gamma = 0$, the solid line is the same solution shown in Fig. 5 with $\gamma = 1$, and the dashed line represents an unstable (i.e., self-oscillating) solution with $\gamma = 1.12$. The solid line phase curve in the lower panel of Fig. 7 has a positive slope at $x = 0$; this indicates that the traveling-wave propagation is directed outward at the stapes. In other words, the cochlear is *emitting* sound for this unstable condition.

The active elements in the model function collectively as a *cochlear amplifier*. We will consider two ways of defining the effective gain of this cochlear amplifier. First, we define *total power gain* as the ratio of the power absorbed by the cochlear partition (over all regions where the driving-point impedance has a positive real part) relative to the power input at the stapes; this ratio, when expressed in decibels, is positive whenever the active elements are contributing energy to the cochlear fluid. The total power gain is about 45 dB at 25.6 kHz and about 6 dB at 0.4 kHz for the model parameters used in this paper. In other words, the mechanical energy provided by the active elements is about 30 000 times as much as that provided by the middle ear at 25.6 kHz and about three times as much at 0.4 kHz. Another measure of gain is the ratio of the amplitude of BM displacement at the place of maximum response at a given frequency in the active model to the amplitude at the same place and frequency in the passive model. In the upper panel to Fig. 8, we can see that the amplitude gain of the cochlear amplifier is about 63

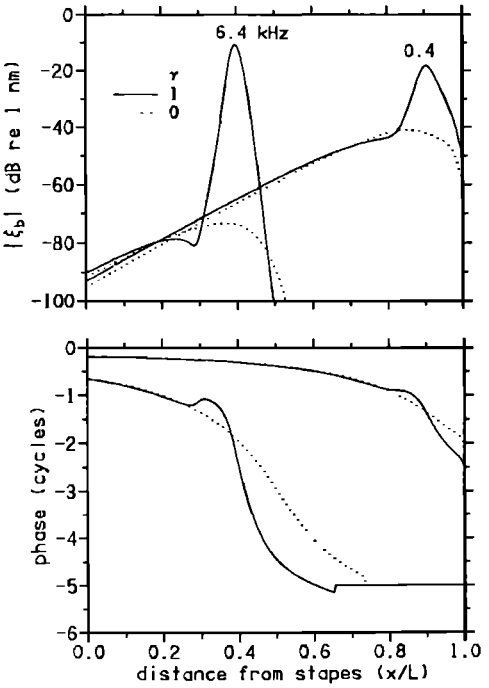

FIG. 8. Effect of active elements on basilar membrane displacement ξ_b at two different frequencies. The dotted line represents a "passive" cochlea with $\gamma = 0$ and the solid line represents a "normal" cochlea with $\gamma = 1$. The difference in magnitude between the "active" and "passive" cases at the characteristic place is 63 dB at 6.4 kHz and 24 dB at 0.4 kHz.

dB at 6.4 kHz and about a 24 dB at 0.4 kHz. It is clear from either definition of gain that the cochlear amplifier has a very *significant influence at high* frequencies and much less influence at low frequencies.

IV. COMPARISON BETWEEN MEASUREMENTS AND MODEL

In this section we compare *in vivo* measurements of cochlear mechanics with solutions of our cochlear model.

Figure 9 shows the mapping between frequency and place for hair cell excitation ξ_c. The dashed line is from Liberman (1982) obtained by labeling single nerve fibers after determining the characteristic frequency (CF) of the fiber and tracing the fiber histologically to determine its place of innervation. The solid line is obtained by solving the frequency-domain model for many different frequencies and determining the characteristic place for each frequency. The slope of the frequency-place map is more constant for the model than for Liberman's data because most of the model parameters are constrained to have exponential dependence on x.

In Fig. 10, the dashed lines represent the response of a population of auditory nerve fibers to tones at 0.62 and 1.55 kHz as a function of the fiber's CF (Kim *et al.*, 1979). The solid lines show model solutions for hair bundle displacement at these frequencies. To compare the model solutions with the neural data the model results are transformed in the following ways: (1) place for the model solutions is transformed into CF using a straight line approximation to the frequency-place map shown in Fig. 9; (2) a displacement magnitude of 0.05 nm is plotted at the same vertical position as spontaneous rate; and (3) the phase lag has been increased by 1.2 ms to account for acoustic and synaptic propagation delay present in the neural data. It is of special interest in this figure that the inflection in the phase curves toward leading phase, clearly seen in the neural data, is also present in the model data. The amplitude curves for model

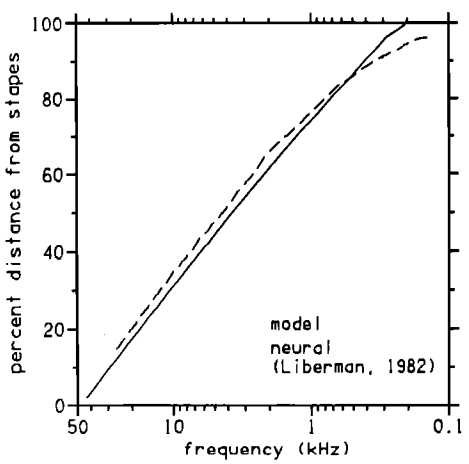

FIG. 9. Cochlear frequency-place map. The dashed line is a fit to data of Liberman (1982) determined by labeling auditory nerve fibers of known frequency in cat. The solid line shows the place of maximum hair bundle displacement $|\xi_c|$ for solutions of the model at many different frequencies.

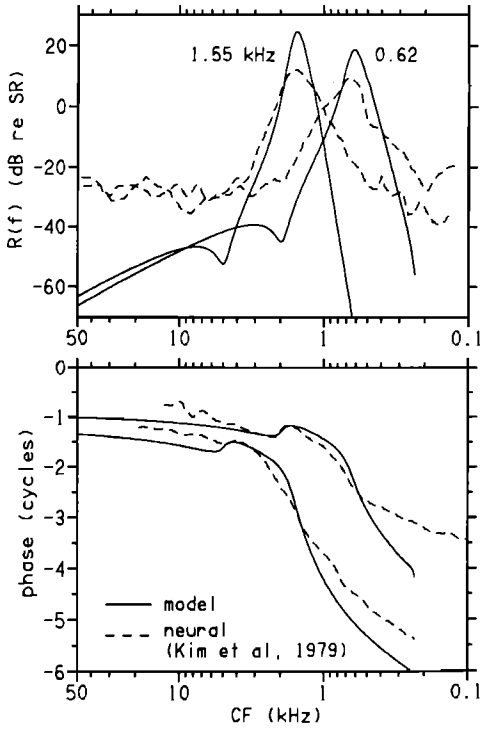

FIG. 10. Comparison between the response of a population of nerve fibers and ξ_c in the model. The dashed curves represent a moving window average of a measure of the response of hundreds of auditory nerve fibers for two stimulus frequencies (0.62 and 1.55 kHz) plotted as a function of the characteristic frequency (CF) of the fiber, from Kim *et al.* (1979). The measure of neural response $R(f)$ is the stimulus frequency component of the Fourier transform of a period histogram of nerve spike discharge in dB re spontaneous rate (SR). The solid lines represent solutions of the model for ξ_c for the same two frequencies. The model data is transformed in three ways to facilitate comparison (1) the x axis is mapped to CF using a straight line fit to the frequency-place map in Fig. 9, (2) a displacement of 0.05 nm is plotted at the same vertical position as SR, (3) the phase lag is increased by an amount corresponding to 0.2 ms delay to account for acoustic and neural propagation delay present in the neural data.

displacement in the upper panel do not include the *nonlinear* effects of neural rate saturation for large displacements or spontaneous neural rate for small displacements. This should be kept in mind when comparing the model curves with the measured neural data.

Figure 11 compares basilar membrane iso-displacement curves for a 1-nm amplitude criterion as a function of frequency. In the upper panel, the curves are based on *in vivo* measurements of three different groups of researchers in three different species. The dotted line represents data of Rhode (1978) from a squirrel monkey using a Mössbauer technique. The dashed line represents data of Khanna and Leonard (1982) from a cat using a laser interference technique. The solid lines in the upper panel represent data of Sellick *et al.* (1982) from a guinea pig using an improved Mössbauer technique. The three curves of Sellick *et al.* show a progressive decline in the sensitivity and sharpness of tuning as the physiological condition of the animal deteriorated. The three curves in the lower panel represent solutions of the model for three values of OHC force-generation gain: $\gamma = 1$, $\gamma = 0.8$, and $\gamma = 0$. The progressive decline in the sensitivity and sharpness of tuning in the model data is similar to that

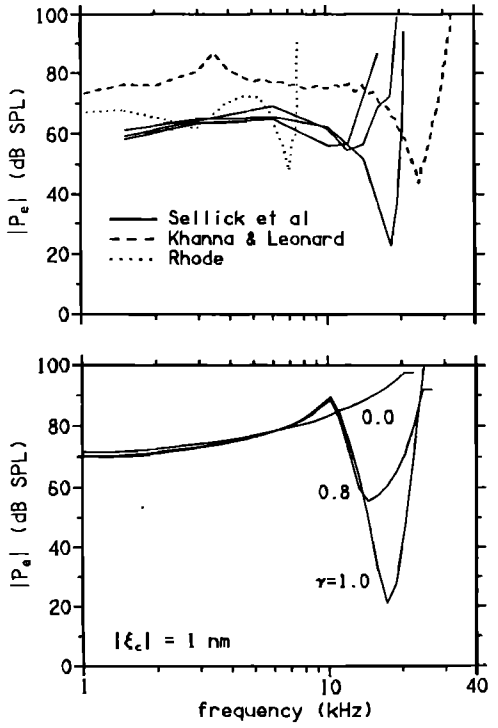

FIG. 11. Comparison between basilar membrane isodisplacement measurements and ξ_b in the model. The upper panel shows *in vivo* measurements of the sound pressure at the eardrum required to achieve 1-nm displacement of the basilar membrane in three different animal species. The dotted lines represent squirrel monkey data (Rhode, 1978), the dashed lines represent cat data (Khanna and Leonard, 1982), and the solid lines represent guinea pig data (Sellick *et al.*, 1982). The lower panel shows similar 1-nm isodisplacement curves for hair bundle displacement $|\xi_c|$ for three different values of transduction gain: $\gamma = 1, 0.8, 0$.

shown above for the *in vivo* data of Sellick *et al.*

Figure 12 compares rate threshold in single auditory nerve fibers with isodisplacement of hair cell excitation ξ_c. The upper panel shows the rate threshold for four auditory nerve fibers from one cat as a function of frequency using as a criterion 1 spike increase in 50 ms above spontaneous rate. The lower panel show 1-nm isodisplacement of ξ_c in the model at four places: $x/L = 0.23, 0.50, 0.75$, and 0.90.

In Fig. 13 we show the effect on a model tuning curve (isodisplacement of ξ_c) of removing first the active elements P_a and then the stiffness k_3 which couples the OC to the TM. This manipulation of the model parameters is intended to simulate the effects of outer hair cell damage such as that demonstrated by Liberman and Dodds (1984). In our model, removal of P_a (middle panel of Fig. 13) reduces, but does not completely eliminate, the "tip" of the tuning curve. Removal of k_3 (lower panel of Fig. 13) eliminates the remainder of "tip" of the tuning curve and also lowers the "tail" of the tuning curve. The stiffness k_3 restrains shearing motion between the OC and the TM in the same manner as the hair bundles of the OHC; thus, removal of k_3 facilitates the shearing displacement ξ_c.

V. DISCUSSION

The model of cochlear mechanics presented in this paper represents an attempt to bring together several different observations of normal cochlear function into a unified framework based on physical principles. This is not just an exercise in curve fitting. The model provides a means of evaluating and refining hypotheses which are difficult or impossible to test in animal subjects.

The representation of fluid mechanics by only one spatial dimension (1 D) is an important simplification because it greatly reduces the computation needed for numerical solution. The model equations have been formulated to allow straightforward extension to three-dimensional (3-D) fluid mechanics in future versions of the model. The difference between 1-D and 3-D models can be understood in terms of the variation in fluid inertial loading on the cochlear partition as a function of the spatial wavelength of partition displacement (de Boer, 1981; Neely, 1985; Steele and Taber, 1979). The shapes of the tuning curves are somewhat affected by the one-dimensional fluid approximation; the greatest effect is on the high-frequency side of the CF, which corresponds to the apical side of the characteristic place when viewed spatially. To simulate details on the high-frequency side of CF [such as the phase plateau in Rhode's (1978) BM measurements], a 2-D or 3-D model would be more appropriate.

Nonlinear elements have been excluded from the present model for simplicity, but certainly have an important role in cochlear mechanics (e.g., Kim *et al.*, 1980). Nonlinear equations, in general, are more difficult to solve and the results more difficult to interpret. One of the most successful attempts to combine nonlinear and active components in a

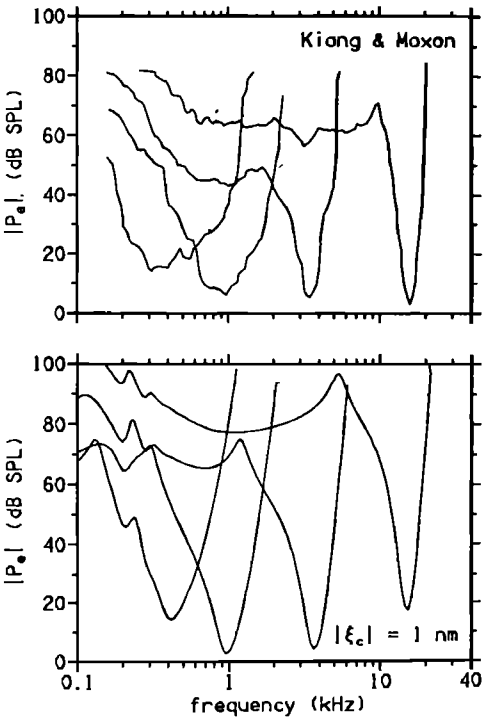

FIG. 12. Comparison between nerve fiber rate-threshold measurements and ξ_c in the model. The curves in the upper panel show threshold of three auditory nerve fibers in a cat (Kiang and Moxon, 1972) using a criterion of 1 spike increase in 50 ms over spontaneous rate (SR). The curves in the lower panel show 1-nm isodisplacement for hair bundle displacement $|\xi_c|$ in the model.

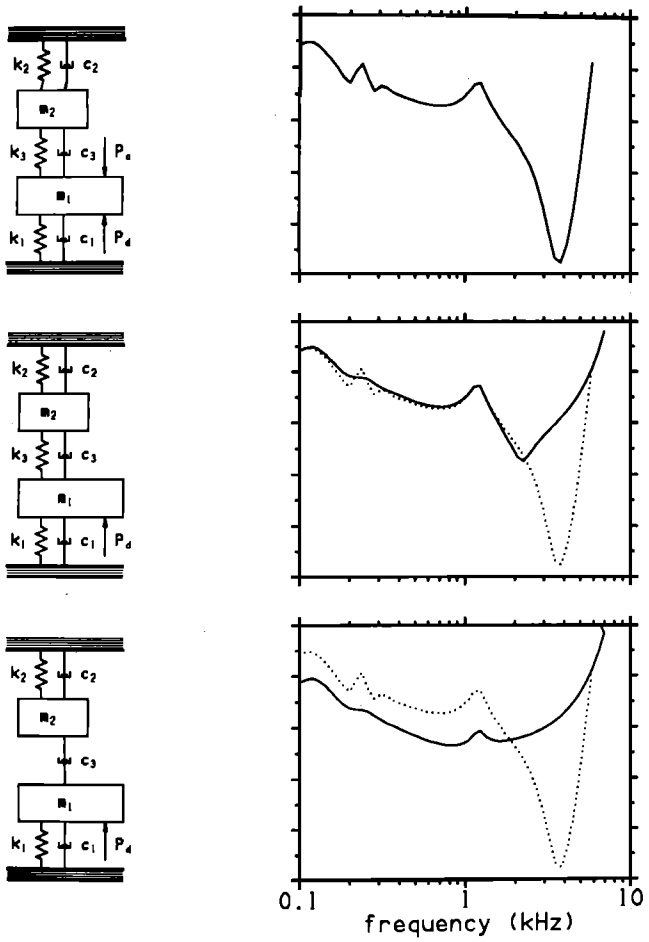

FIG. 13. The effect of removing P_a and k_3 on a high-frequency tuning curve. The upper panel represents the normal state of the model; the tuning curve is a 1-nm isodisplacement curve for ξ_c at $x/L = 0.5$. In the middle panel, the model parameter γ was set to zero to remove the active elements P_a from the entire length of the cochlea. (The solid line is the modified tuning curve and the dotted line is the normal tuning curve.) In the lower panel, the model parameter k_3 was also set to zero.

model of cochlear mechanics is the "hardware" model of Zwicker and Lumer (1986) which uses electrical and electronic components to simulate both active and nonlinear elements in cochlear micromechanics.

In the model equations presented in this paper, the fluid inertial loading on the cochlear partition has been lumped into the mass of the partition. The derivation of the one-dimensional approximation (Neely, 1985) assumes the fluid pressure does not vary in the y or z dimensions and requires that one third of the total fluid mass be added to that of the partition. We found this requirement to conflict with other modeling requirements. We had to use a much smaller mass value to obtain a 50-kHz resonance at the basal end of the partition (Liberman, 1982) without exceeding a 2-MΩ cochlear input impedance (Lynch *et al.*, 1981). This indicates a major weakness in the one-dimensional approximation in the basal region of the cochlea.

The model suggests a role for active elements in the cochlea as an essential part of normal cochlear function. The active elements take the form of a pressure source in this model, but their most important characteristic is that they supply mechanical energy to the cochlea at the expense of electrochemical energy which is readily available in the cochlear endolymph. The physical correspondence of the pressure source and its associated model parameters is not completely defined in this paper because we are uncertain of many important details. The present formulation of the model equations uses P_a to represent a mechanical force generated by the outer hair cells in response to hair bundle displacement. This active force pushes against the surrounding fluid (and not against the TM due to incompressibility of the fluid).

The active elements are bidirectionally coupled to the basilar membrane in a manner such that vibrations of the basilar membrane are *amplified* in a frequency- and place-specific manner. We consider this cochlear amplifier to be directly responsible for the sharp tip seen in typical cochlear tuning curves of high-CF units. The model predicts that most of this sharp tip is also observable in both basilar membrane displacement and fluid pressure difference across the cochlear partition.

Our previous attempts to model cochlear micromechanics with active elements (Neely and Kim, 1983) did not allow any difference between tuning of the basilar membrane and hair bundle displacement. The present model represents an attempt to combine active elements and a "second filter" into a single model of micromechanics. The active elements have greatest influence in the basal region of the cochlea which responds to high frequencies. The energy required to boost cochlear sensitivity at high frequencies is only reasonable at very low sound intensities levels near the threshold of hearing. We expect that at higher sound intensities the force-generation gain should be less than its value at hearing threshold.

One of the key assumptions necessary to compare the mechanical data with neural data is that a neural tuning curve based on spike rate corresponds to a mechanical tuning curve based on *isodisplacement* of the hair bundle instead of *isovelocity*. This assumption is supported by the agreement between the model and neural tuning curves in Fig. 12. The correspondence between model displacement threshold and neural rate threshold is consistent with the possibility that the tips of the tallest stereocilia of IHC are attached to (or in contact with) the TM (Hoshino, 1976). Model results in Fig. 12 suggest that the common "1 spike per 50 ms" rate-threshold criterion corresponds to about 1-nm (peak) hair bundle displacement.

Another interesting aspect of the present model is that it reproduces the inflection in the phase curves toward leading phase in the lower panel of Fig. 10. The phase does not decline monotonically, but shifts by as much as π radians in the leading phase direction in both the neural data and the model data. In the model, this region of leading phase corresponds to the TM contribution ξ_t dominating over the BM contribution ξ_b (Zwislocki, 1983). If this micromechanical model is correct, then perhaps it can be extended to help explain the nonmonotonicities which are often seen in rate *versus* intensity curves (Kiang and Moxon, 1972); the rate-intensity notches may indicate a transition between the dominance of the TM contribution and the BM contribution.

We have attempted, as much as possible, to incorporate into the model both physical principles and experimental observations related to sensitivity and tuning in the cochlear biomechanics. The large energy requirement at high frequencies suggests that, at low sound intensity levels, nearly all the energy required for exciting the IHC may be supplied by the OHC. We intend to refine this model as our understanding of cochlear function improves.

ACKNOWLEDGMENTS

This research was supported, in part, by NIH research grants NS20652, NS19624, and NS18426.

APPENDIX: METHOD FOR NUMERICAL SOLUTION

The one-dimensional model equations described in Secs. I and II result in a tridiagonal matrix equation which can easily be solved by Gaussian elimination. To illustrate the solution method, we will solve for P_d at N discrete positions x_n along the x dimension of the cochlear model

$$x_n = (n-1)\Delta, \tag{A1}$$

where $\Delta = L/(N-1)$ and $n = 1,2,...,N$. We will use a_n and p_n as intermediate variables and start by representing the middle ear influence on the basal boundary conditions

$$a_0 = -2i\omega\rho\Delta A_s/WHZ_m, \tag{A2}$$

$$p_0 = (A_m/G_m A_s)a_0 P_e. \tag{A3}$$

The basal boundary is at the position represented by $n = 1$,

$$a_1 = (1-a_0)^{-1}, \tag{A4}$$

$$p_1 = a_1 p_0. \tag{A5}$$

Then moving toward the apex, $n = 2,...,(N-1)$,

$$z_n = (H/\Delta)Z_p(x_n), \tag{A6}$$

$$a_n = (2 - a_{n+1} + 2i\omega\rho\Delta/z_n)^{-1}, \tag{A7}$$

$$p_n = a_n p_{n-1}. \tag{A8}$$

At the apical boundary, $n = N$,

$$a_N = (1 - a_n + 2i\omega\rho\Delta/c_h)^{-1}, \tag{A9}$$

and

$$P_d(x_N) = a_N p_{N-1}. \tag{A10}$$

Then for $n = (N-1),...,1$,

$$P_d(x_N) = p_n + a_n P_d(x_{n+1}). \tag{A11}$$

Other model variables are computed from P_d. This solution method can be generalized to implement a solution of finite-difference equations for a two-dimensional cochlear model (Neely, 1981), or other similar sets of coupled, second-order differential equations representing three-dimensional fluid motion (Neely, 1985).

Allen, J. B. (1977). "Two-dimensional cochlear fluid model: New results," J. Acoust. Soc. Am. **61**, 110–119.

Allen, J. B. (1980). "Cochlear micromechanics—A physical model of transduction," J. Acoust. Soc. Am. **68**, 1660–1679.

Brownell, W. E., Bader, C. E., Bertrand, D., and deRibaupierre, Y. (1985). "Evoked mechanical responses of isolated cochlear outer hair cells," Science **227**, 194–196.

Davis, H. (1983). "An active process in cochlear mechanics," Hear. Res. **9**, 1–49.

de Boer, E. (1980). "Auditory Physics. Physical principles in hearing I," Phys. Rep. **62**, 97–274.

deBoer, E. (1981). "Short waves in three-dimensional cochlea models: solution for a 'block' model," Hear. Res. **4**, 53–77.

deBoer, E. (1984). "Auditory Physics. Physical principles in hearing II," Phys. Rep. **105**, 141–226.

Guinan, J. J., and Peake, W. T. (1967). "Middle-ear characteristics of anesthetized cats," J. Acoust. Soc. Am. **41**, 1237–1261.

Hoshino, T. (1976). "Attachment of inner sensory hair cells to the tectorial membrane. A scanning electron microscope study," Ann. Otol. Rhinol. Laryngol. **38**, 115–123.

Hudspeth, A. J., and Corey, D. P. (1977). "Sensitivity, polarity, and conductance change in the response of vertebrate hair cells to controlled mechanical stimuli," Proc. Natl. Acad. Sci. (USA) **74**, 2407–2411.

Khanna, S. M., and Leonard, D. G. B. (1982). "Basilar membrane tuning in the cat cochlea," Science **215**, 305–306.

Kiang, N. Y. S., and Moxon, E. C. (1972). "Physiological considerations in artificial stimulation of the inner ear," Ann. Otol. Rhinol. Laryngol. **81**, 714–730.

Kim, D. O., Siegel, J. H., and Molnar, C. E. (1979). "Cochlear nonlinearities in two-tone responses," Scand. Audio. Suppl. **9**, 63–81.

Kim, D. O., Neely, S. T., Molnar, C. E., and Matthews, J. W. (1980). "An active cochlear model with negative damping in the cochlear partition: Comparison with Rhode's ante- and post-mortem results," in *Psychological, Physiological, and Behavioral Studies in Hearing*, edited by G. van den Brink and F. A. Bilsen (Delft U. P., Delft, The Netherlands), pp. 7–14.

Liberman, M. C. (1982). "The cochlear frequency map for the cat: Labeling auditory nerve fibers of known characteristic frequency," J. Acoust. Soc. Am. **72**, 1441–1449.

Liberman, M. C., and Dodds, L. W. (1984). "Single-neuron labeling and chronic cochlear pathology. III. Stereocilia damage and alterations to threshold tuning curves," Hear. Res. **16**, 55–74.

Lynch, T. J., Nedzelnitsky, V., and Peake, W. T. (1981). "Input impedance of the cochlea in cat," J. Acoust. Soc. Am. **72**, 108–130.

Neely, S. T. (1981). "Finite difference solution of a two-dimensional cochlear model," J. Acoust. Soc. Am. **69**, 1386–1393.

Neely, S. T., and Kim, D. O. (1983). "An active cochlear model showing sharp tuning and high sensitivity," Hear. Res. **9**, 123–130.

Neely, S. T. (1985). "Mathematical modeling of cochlear mechanics," J. Acoust. Soc. Am. **78**, 345–352.

Pickles, J. O. (1982). *An Introduction to the Physiology of Hearing* (Academic, London).

Rhode, W. S., and Geisler, C. D. (1967). "Model of the displacement between opposing points on the tectorial membrane and reticular lamina," J. Acoust. Soc. Am. **42**, 185–190.

Rhode, W. S. (1978). "Some observations on cochlear mechanics," J. Acoust. Soc. Am. **67**, 1704–1721.

Sellick, P. M., Patuzzi, R., and Johnstone, B. M. (1982). "Measurement of basilar membrane motion in the guinea pig using the Mössbauer technique," J. Acoust. Soc. Am. **72**, 131–141.

Steele, C. R., and Taber, L. A. (1979). "Comparison of WKB calculations and experimental results for three-dimensional cochlear models," J. Acoust. Soc. Am. **65**, 1007–1018.

Viergever, M. A. (1980). *Mechanics of the Inner Ear—A Mathematical Approach* (Delft U. P., Delft, The Netherlands).

Zwicker, E., and Lumer, G. (1986). "Evaluating traveling-wave characteristics in man by an active nonlinear cochlea preprocessing model," in *Peripheral Auditory Mechanisms*, edited by J. B. Allen, J. L. Hall, A. Hubbard, S. T. Neely, and A. Tubis (Springer, Munich).

Zwislocki, J. J. (1950). "Theory of acoustical action in the cochlea," J. Acoust. Soc. Am. **22**, 778–784.

Zwislocki, J. J., and Kletsky, E. J. (1979a). "Micromechanics in the theory of cochlear mechanics," Hear. Res. **2**, 505–512.

Zwislocki, J. J., and Kletsky, E. J. (1979b). "Tectorial membrane: A positive effect on frequency analysis in the cochlea," Science **204**, 639–641.

Zwislocki, J. J. (1983). "What is the response phase of inner hair cells?," Res. Otolaryngol. **6**, 68 (Abs.).